American Journal of Computational Mathematics, 2023, 13, 295-322
https://www.scirp.org/journal/ajcm
ISSN Online: 2161-1211
ISSN Print: 2161-1203

Second-Order MaxEnt Predictive Modelling Methodology. III: Illustrative Application to a Reactor Physics Benchmark

Ruixian Fang, Dan Gabriel Cacuci*

Center for Nuclear Science and Energy, Department of Mechanical Engineering, University of South Carolina, Columbia, SC, USA
Email: fangr@cec.sc.edu, *cacuci@cec.sc.edu

How to cite this paper: Fang, R.X. and Cacuci, D.G. (2023) Second-Order MaxEnt Predictive Modelling Methodology. III: Illustrative Application to a Reactor Physics Benchmark. *American Journal of Computational Mathematics*, **13**, 295-322.
https://doi.org/10.4236/ajcm.2023.132015

Received: April 18, 2023
Accepted: June 18, 2023
Published: June 21, 2023

Copyright © 2023 by author(s) and Scientific Research Publishing Inc.
This work is licensed under the Creative Commons Attribution International License (CC BY 4.0).
http://creativecommons.org/licenses/by/4.0/
Open Access

Abstract

This work illustrates the innovative results obtained by applying the recently developed the 2nd-order predictive modeling methodology called "2nd-BERRU-PM", where the acronym BERRU denotes "best-estimate results with reduced uncertainties" and "PM" denotes "predictive modeling." The physical system selected for this illustrative application is a polyethylene-reflected plutonium (acronym: PERP) OECD/NEA reactor physics benchmark. This benchmark is modeled using the neutron transport Boltzmann equation (involving 21,976 uncertain parameters), the solution of which is representative of "large-scale computations." The results obtained in this work confirm the fact that the 2nd-BERRU-PM methodology predicts best-estimate results that fall in between the corresponding computed and measured values, while reducing the predicted standard deviations of the predicted results to values smaller than either the experimentally measured or the computed values of the respective standard deviations. The obtained results also indicate that 2nd-order response sensitivities must always be included to quantify the need for including (or not) the 3rd- and/or 4th-order sensitivities. When the parameters are known with high precision, the contributions of the higher-order sensitivities diminish with increasing order, so that the inclusion of the 1st- and 2nd-order sensitivities may suffice for obtaining accurate predicted best-estimate response values and best-estimate standard deviations. On the other hand, when the parameters' standard deviations are sufficiently large to approach (or be outside of) the radius of convergence of the multivariate Taylor-series which represents the response in the phase-space of model parameters, the contributions stemming from the 3rd- and even 4th-order sensitivities are necessary to ensure consistency between the computed and measured response. In such cases, the use of only the 1st-order sensitivities erroneously

indicates that the computed results are inconsistent with the respective measured response. Ongoing research aims at extending the 2nd-BERRU-PM methodology to fourth-order, thus enabling the computation of third-order response correlations (skewness) and fourth-order response correlations (kurtosis).

Keywords

Second-Order Predictive Modeling, OECD/NEA Reactor Physics Benchmark, Data Assimilation, Best-Estimate Results, Uncertainty Quantification, Reduced Predicted Uncertainties

1. Introduction

The accompanying works [1] [2] have presented the second-order predictive modelling (acronym: PM) methodology conceived by Cacuci for obtaining "best-estimate results with reduced uncertainties" (acronym: BERRU). This methodology, designated by the acronym "2nd-BERRU-PM," relies fundamentally on the maximum entropy (MaxEnt) principle of thermodynamics [3] and Shannon's information theory [4]. These conceptual underpinnings of the 2nd-BERRU-PM methodology are in contradistinction to the data assimilation methodology [5], which relies on minimizing a subjective user-defined functional which is meant to represent, in the energy-norm, the differences between measured and computed results of interest (called "responses"). As has been presented in [1] [2], there are two complementary methodological frameworks for constructing the 2nd-BERRU-PM methodology, leading to equivalent, but not identical results. One framework is constructed by incorporating the representation of the computational model deterministically; the resulting methodology has been designated by the acronym "2nd-BERRU-PMD" [1], where the letter "D" indicates "deterministic". The alternative framework is constructed by incorporating the representation of the computational model probabilistically; the resulting methodology has been designated by the acronym "2nd-BERRU-PMP" [2], where the last letter of the acronym ("P") indicates "probabilistic".

In this work, the 2nd-BERRU-PMD [1] methodology (which deterministically incorporates the representation of the computational model) will be used to illustrate quantitatively the effects of second- and higher-order sensitivities for obtaining best-estimate results with reduced uncertainties for the polyethylene-reflected plutonium (acronym: PERP) OECD/NEA reactor physics benchmark [6]. This benchmark is modeled using the neutron transport Boltzmann equation, the solution of which is representative of "large-scale computations" and involves a large number (21,976) of uncertain parameters. The Boltzmann forward and adjoint neutron transport equations are solved using the software packages PARTISN [7] and SOURCES4C [8] in conjunction with the MENDF71X [9] cross section data. The characteristics of the PERP benchmark are briefly

presented in Section 2, along with the computational method for solving the Boltzmann transport equation. This equation models the neutron distribution within this benchmark, including the neutron leakage from the outer surface of the benchmark, which will be the "response" of interest in this illustrative application. The specific particular forms taken on by the 2nd-BERRU-PMD [1] mathematical formulas for the best-estimate predicted results (responses) along with the corresponding reduction in the accompanying predicted standard deviation will also be presented in Section 2. The numerical results produced by the 2nd-BERRU-PMD [1] will be presented in Section 3, highlighting the essential impact and contributions of the 2nd-, 3rd- and 4th-order sensitivities on the results. In particular, it is shown in Section 3 that mistaken indications of inconsistency between measurements and computations—when only 1st-order sensitivities are considered—are actually corrected to the contrary by the inclusion of higher-order sensitivities (*i.e.*, using only 1st-order sensitivities indicates that the computations are inconsistent with the measurements, but the contrary becomes apparent when the contributions from the higher-order sensitivities are included). The discussion in Section 4 of the significance of the 2nd-BERRU-PM methodology, as illustrated by using the PERP reactor physics benchmark, concludes this work.

2. Methods

This Section illustrates the steps involved in applying the 2nd-BERRU-PMD methodology [1] to the spherical polyethylene-reflected plutonium (acronym: PERP) OECD/NEA reactor physics benchmark [6]. This benchmark is modeled using the neutron transport equation, the solution of which is representative of "large-scale computations" and involves a large number (21,976) of uncertain parameters. The PERP benchmark comprises a metallic inner sphere ("core") containing the following 4 isotopes: Isotope 1 (239Pu), Isotope 2 (240Pu), Isotope 3 (69Ga) and Isotope 4 (71Ga). This core (which is designated as "material 1") is surrounded by a spherical shell of polyethylene (designated as "material 2"), containing two isotopes, designated as Isotope 5 (C) and Isotope 6 (1H), respectively. The characteristics of the PERP benchmark are presented in **Table 1**, below.

The neutron flux distribution within the PERP benchmark, as well as the leakage of neutrons out of the benchmark's outer surface, has been modeled using the standard multigroup form of the Boltzmann neutron transport equation with an internal spontaneous fission source, and subject to the boundary condition of no incoming flux, which can be written in the following matrix-form:

$$\boldsymbol{B}(\boldsymbol{\alpha})\boldsymbol{\varphi}(r,\boldsymbol{\Omega})=\boldsymbol{Q}(\boldsymbol{c}),\ \ \boldsymbol{\varphi}(r,\boldsymbol{\Omega})=\boldsymbol{0},\ \ r=r_d,\ \boldsymbol{\Omega}\cdot\boldsymbol{n}<0. \tag{1}$$

The quantities appearing in Equation (1) are defined as follows: r_d denotes the radius of the PERP sphere; the matrix $\boldsymbol{B}(\boldsymbol{\alpha})$ and the vectors $\boldsymbol{Q}(\boldsymbol{\alpha})$ and $\boldsymbol{\varphi}(r,\boldsymbol{\Omega})$ are defined as follows:

$$\boldsymbol{B}(\boldsymbol{\alpha}) \triangleq \begin{pmatrix} B_{11}(\boldsymbol{\alpha}) & \cdot & B_{1g}(\boldsymbol{\alpha}) & \cdot & B_{1G}(\boldsymbol{\alpha}) \\ \cdot & \cdot & \cdot & \cdot & \cdot \\ B_{g1}(\boldsymbol{\alpha}) & \cdot & B_{gg}(\boldsymbol{\alpha}) & \cdot & B_{gG}(\boldsymbol{\alpha}) \\ \cdot & \cdot & \cdot & \cdot & \cdot \\ B_{G1}(\boldsymbol{\alpha}) & \cdot & B_{Gg}(\boldsymbol{\alpha}) & \cdot & B_{GG}(\boldsymbol{\alpha}) \end{pmatrix}; \ \boldsymbol{\varphi}(r,\boldsymbol{\Omega}) \triangleq \begin{pmatrix} \varphi^1 \\ \cdot \\ \varphi^g \\ \cdot \\ \varphi^G \end{pmatrix}; \ \boldsymbol{Q}(\boldsymbol{\alpha}) \triangleq \begin{pmatrix} Q^1 \\ \cdot \\ Q^g \\ \cdot \\ Q^G \end{pmatrix}; \quad (2)$$

having components defined below:

$$\begin{aligned} &B_{gh}(\boldsymbol{\alpha}) \triangleq \delta_{g,h} B^0_{gg}(\boldsymbol{\alpha}) - B^1_{gh}(\boldsymbol{\alpha}); \ g,h = 1,\cdots,G; \\ &B^0_{gg}(\boldsymbol{\alpha})\varphi^g(r,\boldsymbol{\Omega}) \triangleq \left[\boldsymbol{\Omega}\cdot\nabla + \Sigma^g_t(\boldsymbol{\alpha};r)\right]\varphi^g(r,\boldsymbol{\Omega}); \\ &B^1_{gh}(\boldsymbol{\alpha})\varphi^h(r,\boldsymbol{\Omega}') \triangleq \int_{4\pi} \mathrm{d}\boldsymbol{\Omega}' \left[\Sigma^{h\to g}_s(\boldsymbol{\alpha};r,\boldsymbol{\Omega}'\to\boldsymbol{\Omega}) + \chi^g(\boldsymbol{\alpha};r)\left(\nu\Sigma_f\right)^h(\boldsymbol{\alpha};r)\right]; \end{aligned} \quad (3)$$

$$Q^g(\boldsymbol{c}) \triangleq \sum_{k=1}^{N_f} \lambda_k N_k F_k^{SF} \nu_k^{SF} \left(\frac{2}{\sqrt{\pi a_k^3 b_k}} \mathrm{e}^{-\frac{a_k b_k}{4}}\right) \int_{E^{g+1}}^{E^g} \mathrm{d}E\, \mathrm{e}^{-E/a_k} \sinh\sqrt{b_k E}\,. \quad (4)$$

The notation $\delta_{g,h}$, which appears in Equation (3), denotes the Kronecker delta-functional, which is defined as usual, *i.e.*, $\delta_{g,h} = 1$, if $g = h$ and $\delta_{g,h} = 0$, if $g \neq h$. The quantities appearing in Equations (1)-(4) are defined as follows:

1) The quantity $\varphi^g(r,\boldsymbol{\Omega})$ is the customary "group-flux" for group *g*, $g = 1,\cdots,G$.

2) The source $Q^g(\boldsymbol{c})$ depends on the vector of model parameters $\boldsymbol{c}$, defined as follows:

$$\boldsymbol{c} \triangleq \left[c_1,\cdots,c_{JQ}\right]^\dagger \triangleq \left[\lambda_1,\lambda_2;F_1^{SF},F_2^{SF};a_1,a_2;b_1,b_2;\nu_1^{SF},\nu_2^{SF}\right]^\dagger, \ JQ = 10. \quad (5)$$

3) As indicated in **Table 1**, the PERP benchmark comprises 2 materials: "material 1" comprises 4 isotopes, numbered 1 through 4, while "material 2" comprises 2 isotopes, numbered 5 and 6. These materials contain only isotopes that are distinct from each other, so the atomic number density N_i of an isotope *i*, $i = 1,\cdots,I = 6$, is computed as follows:

$$N_i = \frac{\rho_1 w_{i,1} N_A}{A_i}; \text{ for } i = 1,2,3,4; \ N_i = \frac{\rho_2 w_{i,2} N_A}{A_i}; \text{ for } i = 5,6, \quad (6)$$

where ρ_m denotes the mass density of material *m*, $m = 1,2$; $w_{i,m}$ denotes the weight fraction of isotope *i* in material *m*; A_i denotes the atomic weight of

Table 1. Dimensions and material composition of the PERP benchmark.

Materials	Isotopes	Weight Fraction	Density (g/cm³)	Zones
Material 1 (plutonium metal)	Isotope 1 (^{239}Pu)	9.3804×10^{-1}	19.6	Homogeneous sphere of radius $r_1 = 3.794$ cm, designated as "material 1" and assigned to zone 1
	Isotope 2 (^{240}Pu)	5.9411×10^{-2}		
	Isotope 3 (^{69}Ga)	1.5152×10^{-3}		
	Isotope 4 (^{71}Ga)	1.0346×10^{-3}		
Material 2 (polyethylene)	Isotope 5 (C)	8.5630×10^{-1}	0.95	Homogeneous spherical shell of inner radius $r_1 = 3.794$ cm and outer radius $r_2 = 7.604$ cm, designated as "material 2" and assigned to zone 2
	Isotope 6 (^{1}H)	1.4370×10^{-1}		

isotope *i*; N_A denotes Avogadro's number. The atomic number densities N_i, $i=1,\cdots,I=6$ will be considered to be components of the vector denoted as $\boldsymbol{N}$ and defined as follows: $\boldsymbol{N} \triangleq \left[N_1, N_2, N_3, N_4, N_5, N_6\right]^\dagger$.

4) The scattering transfer cross section from energy group g', $g'=1,\cdots,G$, into energy group *g*, $g=1,\cdots,G$, is denoted as $\Sigma_s^{g'\to g}\left(\boldsymbol{\alpha};r,\boldsymbol{\Omega}'\to\boldsymbol{\Omega}\right)$ and is computed in terms of the *l*-th order Legendre coefficient $\sigma_{s,l,i}^{g'\to g}$ using the following 3rd-order expansion in Legendre functions :

$$\Sigma_s^{g'\to g}\left(\boldsymbol{\alpha};r,\boldsymbol{\Omega}'\to\boldsymbol{\Omega}\right)=\sum_{i=1}^{I=6}N_i\sum_{l=0}^{ISCT=3}\left(2l+1\right)\sigma_{s,l,i}^{g'\to g}P_l\left(\boldsymbol{\Omega}'\cdot\boldsymbol{\Omega}\right),\ g,g'=1,\cdots,G, \quad (7)$$

where $ISCT=3$ denotes the order of the expansion in Legendre polynomials. The microscopic scattering cross sections $\sigma_{s,l,i}^{g'\to g}$ for isotope *i*, and from energy group g' into energy group *g*, are tabulated parameters. The zeroth-order (*i.e.*, $l=0$) scattering cross sections must be considered separately from the higher order (*i.e.*, $l\geq 1$) scattering cross sections, since the former contribute to the total cross sections (as noted below), while the latter do not. The microscopic scattering cross sections $\sigma_{s,l,i}^{g'\to g}$ will be considered to be components of a vector $\boldsymbol{\sigma}_s$ defined below:

$$\begin{aligned}&\boldsymbol{\sigma}_s \triangleq \left[s_1,\cdots,s_{JSX}\right]^\dagger\\ &\triangleq\left[\sigma_{s,l=0,i=1}^{g'=1\to g=1},\sigma_{s,l=0,i=1}^{g'=2\to g=1},\cdots,\sigma_{s,l=0,i=1}^{g'=G\to g=1},\sigma_{s,l=0,i=1}^{g'=1\to g=2},\sigma_{s,l=0,i=1}^{g'=2\to g=2},\cdots,\sigma_{s,l,i}^{g'\to g},\cdots,\sigma_{s,ISCT,i=I}^{G\to G}\right]^\dagger,\\ &l=0,\cdots,ISCT;\ i=1,\cdots,I;\ g,g'=1,\cdots,G;\ JSX=\left(G\times G\right)\times I\times\left(ISCT+1\right).\end{aligned} \quad (8)$$

5) The software package PARTISN [7] computes the quantity $\left(\nu\Sigma_f\right)^g\left(\boldsymbol{\alpha};r\right)$ for each isotope *i* and energy group *g*, as follows:

$$\left(\nu\Sigma_f\right)^g\left(\boldsymbol{\alpha};r\right)=\sum_{i=1}^{N_f=2}N_i\sigma_{f,i}^g\nu_i^g,\ g=1,\cdots,G=30, \quad (9)$$

where $\sigma_{f,i}^g$ denotes the microscopic fission cross section for isotope *i* and energy group *g*, ν_i^g denotes the average number of neutrons per fission for isotope *i* and energy group *g*, and N_f denotes the total number of fissionable isotopes.

$$\begin{aligned}&\boldsymbol{\sigma}_f \triangleq\left[\sigma_{f,i=1}^1,\sigma_{f,i=1}^2,\cdots,\sigma_{f,i=1}^G,\cdots,\sigma_{f,i}^g,\cdots,\sigma_{f,i=NF}^1,\cdots,\sigma_{f,i=NF}^G\right]^\dagger\triangleq\left[f_1,\cdots,f_{JFX}\right]^\dagger,\\ &i=1,\cdots,NF;\ g=1,\cdots,G;\ JFX=G\times NF;\end{aligned} \quad (10)$$

$$\begin{aligned}&\boldsymbol{\nu}\triangleq\left[\nu_{i=1}^1,\nu_{i=1}^2,\cdots,\nu_{i=1}^G,\cdots,\nu_i^g,\cdots,\nu_{i=N_f}^1,\cdots,\nu_{i=NF}^G\right]^\dagger\triangleq\left[f_{JFX+1},\cdots,f_{JFX+JNU}\right]^\dagger,\\ &i=1,\cdots,NF;\ g=1,\cdots,G;\ JNU=G\times NF.\end{aligned} \quad (11)$$

6) The total cross section for energy group *g*, $g=1,\cdots,G$, is denoted as $\Sigma_t^g\left(\boldsymbol{\alpha}\right)$ and is computed using the following expression:

$$\Sigma_t^g\left(\boldsymbol{\alpha}\right)=\sum_{i=1}^I N_i\sigma_{t,i}^g;\ \sigma_{t,i}^g=\left[\sigma_{f,i}^g+\sigma_{c,i}^g+\sum_{g'=1}^G\sigma_{s,l=0,i}^{g\to g'}\right], \quad (12)$$

where the quantities $\sigma_{t,i}^g$, $\sigma_{f,i}^g$ and $\sigma_{c,i}^g$ denote, respectively, the total microscopic cross section, the tabulated group microscopic fission, and the neutron

capture cross sections for isotope i and group g. Other nuclear reactions in the PERP benchmark are negligible. To reduce as much as possible the proliferation of indices when determining the higher-order (up to and including the 4th-order) sensitivities of the PERP leakage response, it is useful to consider that the cross sections $\sigma_{t,i}^{g}$ are the components of a vector $\boldsymbol{t}$, having $JTX \triangleq G \times I$ components defined as follows:

$$\begin{aligned} &\boldsymbol{t} \triangleq \left[t_1, \cdots, t_{JTX}\right]^{\dagger} \triangleq \left[\sigma_{t,i=1}^{1}, \sigma_{t,i=1}^{2}, \cdots, \sigma_{t,i=1}^{G}, \cdots, \sigma_{t,i}^{g}, \cdots, \sigma_{t,i=I}^{1}, \cdots, \sigma_{t,i=I}^{G}\right]^{\dagger}, \\ &\text{for } i = 1, \cdots, I = 6;\ g = 1, \cdots, G = 30;\ JTX \triangleq I \times G. \end{aligned} \tag{13}$$

7) The quantity $\chi^{g}(\boldsymbol{\alpha}; r)$ quantifies the fission spectrum in energy group g. The fission spectrum is considered to depend on the vector of parameters $\boldsymbol{p}$, defined as follows:

$$\begin{aligned} &\boldsymbol{p} \triangleq \left[p_1, \cdots, p_{J\chi}\right]^{\dagger} \triangleq \left[\chi_{i=1}^{g=1}, \chi_{i=1}^{g=2}, \cdots, \chi_{i=1}^{G}, \cdots, \chi_{i}^{g}, \cdots, \chi_{NF}^{G}\right]^{\dagger}, \\ &\text{for } i = 1, \cdots, NF;\ g = 1, \cdots, G;\ J\chi = G \times NF. \end{aligned} \tag{14}$$

In summary, the model parameters characterizing the PERP benchmark can all be considered to be the components of a "vector of model parameters" denoted as $\boldsymbol{\alpha} \triangleq \left[\alpha_1, \cdots, \alpha_{TP}\right]^{\dagger}$, where the subscript "TP" stands for "Total number of model and response Parameters", and is defined below:

$$\begin{aligned} &\boldsymbol{\alpha} \triangleq \left[\alpha_1, \cdots, \alpha_{TP}\right]^{\dagger} \triangleq \left[\boldsymbol{c}; \boldsymbol{N}; \boldsymbol{\sigma}_s; \boldsymbol{\sigma}_t; \boldsymbol{\sigma}_f; \boldsymbol{\nu}; \boldsymbol{p}\right]^{\dagger}, \\ &\text{where } TP \triangleq JQ + I + JSX + JTX + JFX + JNU + J\chi. \end{aligned} \tag{15}$$

The multigroup Boltzmann (forward and adjoint) neutron transport equation was solved numerically using the software packages PARTISN [7] and SOURCES-4C [8] in conjunction with the MENDF71X [9] 618-group cross section data collapsed to $G = 30$ energy groups, as well as a P3 Legendre expansion of the scattering cross section and a fine-mesh spacing of 0.005 cm (comprising 759 meshes for the plutonium sphere of radius of 3.794 cm, and 762 meshes for the polyethylene shell of thickness of 3.81 cm). The first- and second-order response sensitivities were computed using an angular quadrature of S256. The 3rd- and 4th-order sensitivities of the leakage response with respect to the total cross sections were computed using an angular quadrature of S32. The scattering and fission terms in Equation (1) contain implicitly a factor $1/4\pi$. The group boundaries of the $G = 30$ energy groups are provided in **Table 2**.

Thus, the numerical model of the PERP benchmark comprises 21,976 uncertain parameters, as follows: 180 group-averaged total microscopic cross sections, 21,600 group-averaged scattering microscopic cross sections; 120 fission process parameters; 60 fission spectrum parameters; 10 parameters describing the experiment's nuclear sources; and 6 isotopic number densities.

The quantity of interest in this work, which will be called the "response," is the leakage of neutrons through the outer surface of the spherical benchmark; this leakage response is denoted as $L(\boldsymbol{\alpha})$ and is defined below:

$$L(\boldsymbol{\alpha}) \triangleq \int_{S_b} \mathrm{d}S \sum_{g=1}^{G} \int_{\boldsymbol{\Omega}\cdot\boldsymbol{n}>0} \mathrm{d}\boldsymbol{\Omega}\, \boldsymbol{\Omega} \cdot \boldsymbol{n} \varphi^{g}(r, \boldsymbol{\Omega}). \tag{16}$$

Table 2. Group boundaries, E^g [MeV], of the $G=30$ energy groups used in the PARTISN forward and adjoint neutron transport computations.

g	1	2	3	4	5	6
E^g	1.50×10^{1}	1.35×10^{1}	1.20×10^{1}	1.00×10^{1}	7.79×10^{0}	6.07×10^{0}
E^{g-1}	1.70×10^{1}	1.50×10^{1}	1.35×10^{1}	1.20×10^{1}	1.00×10^{1}	7.79×10^{0}
g	7	8	9	10	11	12
E^g	3.68×10^{0}	2.87×10^{0}	2.23×10^{0}	1.74×10^{0}	1.35×10^{0}	8.23×10^{-1}
E^{g-1}	6.07×10^{0}	3.68×10^{0}	2.87×10^{0}	2.23×10^{0}	1.74×10^{0}	1.35×10^{0}
g	13	14	15	16	17	18
E^g	5.00×10^{-1}	3.03×10^{-1}	1.84×10^{-1}	6.76×10^{-2}	2.48×10^{-2}	9.12×10^{-3}
E^{g-1}	8.23×10^{-1}	5.00×10^{-1}	3.03×10^{-1}	1.84×10^{-1}	6.76×10^{-2}	2.48×10^{-2}
g	19	20	21	22	23	24
E^g	3.35×10^{-3}	1.24×10^{-3}	4.54×10^{-4}	1.67×10^{-4}	6.14×10^{-5}	2.26×10^{-5}
E^{g-1}	9.12×10^{-3}	3.35×10^{-3}	1.24×10^{-3}	4.54×10^{-4}	1.67×10^{-4}	6.14×10^{-5}
g	25	26	27	28	29	30
E^g	8.32×10^{-6}	3.06×10^{-6}	1.13×10^{-6}	4.14×10^{-7}	1.52×10^{-7}	1.39×10^{-10}
E^{g-1}	2.26×10^{-5}	8.32×10^{-6}	3.06×10^{-6}	1.13×10^{-6}	4.14×10^{-7}	1.52×10^{-7}

For convenient reference, the histogram plot of the leakage for each energy group for the PERP benchmark is presented in **Figure 1**, below. The value of the total leakage computed using Equation (16) for the PERP benchmark is 1.7648 × 106 neutrons/sec.

As generally presented in [10], the formulas/expressions used for computing the mean value and the variance of the leakage response are based on the Taylor series of the leakage response around the expected (nominal) parameter values $\boldsymbol{\alpha}^0$, which has the following form up to fourth-order:

$$\begin{aligned} L(\boldsymbol{\alpha}) = L(\boldsymbol{\alpha}^0) &+ \sum_{j_1=1}^{TP}\left\{\frac{\partial L(\boldsymbol{\alpha})}{\partial \alpha_{j_1}}\right\}_{\boldsymbol{\alpha}^0}\delta\alpha_{j_1} + \frac{1}{2}\sum_{j_1=1}^{TP}\sum_{j_2=1}^{TP}\left\{\frac{\partial^2 L(\boldsymbol{\alpha})}{\partial \alpha_{j_1}\partial \alpha_{j_2}}\right\}_{\boldsymbol{\alpha}^0}\delta\alpha_{j_1}\delta\alpha_{j_2} \\ &+ \frac{1}{3!}\sum_{j_1=1}^{TP}\sum_{j_2=1}^{TP}\sum_{j_3=1}^{TP}\left\{\frac{\partial^3 L(\boldsymbol{\alpha})}{\partial \alpha_{j_1}\partial \alpha_{j_2}\partial \alpha_{j_3}}\right\}_{\boldsymbol{\alpha}^0}\delta\alpha_{j_1}\delta\alpha_{j_2}\delta\alpha_{j_3} \\ &+ \frac{1}{4!}\sum_{j_1=1}^{TP}\sum_{j_2=1}^{TP}\sum_{j_3=1}^{TP}\sum_{j_4=1}^{TP}\left\{\frac{\partial^4 L(\boldsymbol{\alpha})}{\partial \alpha_{j_1}\partial \alpha_{j_2}\partial \alpha_{j_3}\partial \alpha_{j_4}}\right\}_{\boldsymbol{\alpha}^0}\delta\alpha_{j_1}\delta\alpha_{j_2}\delta\alpha_{j_3}\delta\alpha_{j_4} + \varepsilon_k. \end{aligned} \tag{17}$$

The radius/domain of convergence of the series in Equation (17) determines the largest values of the parameter variations $\delta\alpha_j$ which are admissible before the respective series becomes divergent.

Considering that the model parameters underlying the PERP benchmark are uncorrelated and normally distributed, and considering only the unmixed higher-order sensitivities, the computed mean value and, respectively, computed

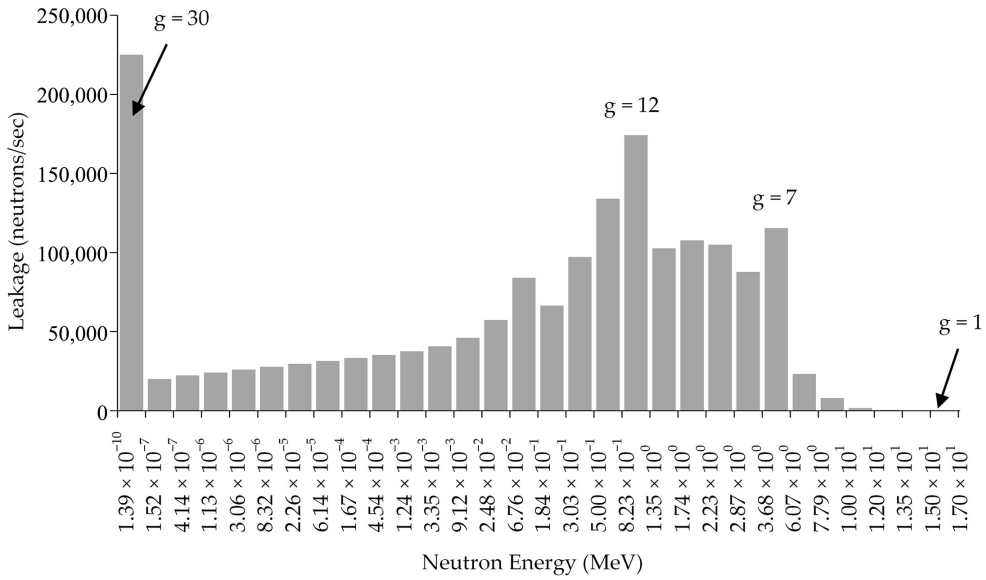

Figure 1. Histogram plot of the leakage for each energy group for the PERP benchmark.

variance of the leakage response have the following expressions [11] when the sensitivities up to fourth-order are included:

$$E\left(L^c\right)=L^c\left(\boldsymbol{\alpha}^0\right)+\frac{1}{2}\sum_{j_1=1}^{TP}\frac{\partial^2 L\left(\boldsymbol{\alpha}^0\right)}{\left(\partial\alpha_{j_1}\right)^2}\sigma_{j_1}^2+\frac{1}{8}\sum_{j_1=1}^{TP}\frac{\partial^4 L\left(\boldsymbol{\alpha}^0\right)}{\left(\partial\alpha_{j_1}\right)^4}\sigma_{j_1}^4, \tag{18}$$

where $L^c\left(\boldsymbol{\alpha}^0\right)=1.7648\times10^6$ neutrons/sec denotes the value of the computed leakage response at the nominal parameter values and where $TP=21976$ denotes the "total number of model parameters."

The computed variance of the leakage response, $\operatorname{var}\left(L^c\right)$, has the following expression [11] when considering only the unmixed response sensitivities to uncorrelated and normally distributed parameters:

$$\begin{aligned}\operatorname{var}\left(L^c\right)=&\sum_{j_1=1}^{TP}\left[\frac{\partial L\left(\boldsymbol{\alpha}^0\right)}{\partial\alpha_{j_1}}\right]^2\sigma_{j_1}^2+\frac{1}{2}\sum_{j_1=1}^{TP}\left[\frac{\partial^2 L\left(\boldsymbol{\alpha}^0\right)}{\left(\partial\alpha_{j_1}\right)^2}\right]^2\sigma_{j_1}^4\\&+\sum_{j_1=1}^{TP}\left[\frac{\partial^3 L\left(\boldsymbol{\alpha}^0\right)}{\left(\partial\alpha_{j_1}\right)^3}\times\frac{\partial L\left(\boldsymbol{\alpha}^0\right)}{\partial\alpha_{j_1}}\right]\sigma_{j_1}^4+\frac{15}{36}\sum_{j_1=1}^{TP}\left[\frac{\partial^3 L\left(\boldsymbol{\alpha}^0\right)}{\left(\partial\alpha_{j_1}\right)^3}\right]^2\sigma_{j_1}^6\\&+\frac{1}{2}\sum_{j_1=1}^{TP}\left[\frac{\partial^4 L\left(\boldsymbol{\alpha}^0\right)}{\left(\partial\alpha_{j_1}\right)^4}\times\frac{\partial^2 L\left(\boldsymbol{\alpha}^0\right)}{\left(\partial\alpha_{j_1}\right)^2}\right]\sigma_{j_1}^6.\end{aligned} \tag{19}$$

The expressions provided in Equations (18) and (19) are valid only if the Taylor series shown in Equation (17) converges. The largest admissible parameter variations $\delta\alpha_j$ which are still within the radius of convergence of Equation (17) provide the largest parameter covariances/standard deviations which can be considered to ensure that the expressions provided in Equations (18) and (19) are valid.

The best-estimate predicted response (leakage) value, denoted as L^{be}, which is obtained after combining the computed response value with a measured response value, is given by the following particular form of the expression derived in [1]:

$$L^{be} = L^e + \operatorname{var}\left(L^e\right)\frac{E\left(L^c\right) - L^e}{\operatorname{var}\left(L^e\right) + \operatorname{var}\left(L^c\right)} = \frac{L^e \operatorname{var}\left(L^c\right) + E\left(L^c\right)\operatorname{var}\left(L^e\right)}{\operatorname{var}\left(L^e\right) + \operatorname{var}\left(L^c\right)}, \quad (20)$$

where: L^e denotes the experimentally measured mean value of the leakage response; $\operatorname{var}\left(L^e\right)$ denotes the experimentally measured variance of the leakage response; $E\left(L^c\right)$ denotes the computed mean value of the leakage response; and $\operatorname{var}\left(L^c\right)$ denotes the computed variance of the leakage response. It is important to note that the relation provided in Equation (20) implies the following inequalities:

$$\text{If } 0 < L^e < E\left(L^c\right), \text{ then } L^e < L^{be} < E\left(L^c\right), \quad (21)$$

$$\text{If } 0 < E\left(L^c\right) < L^e, \text{ then } E\left(L^c\right) < L^{be} < L^e. \quad (22)$$

The inequalities shown in Equations (21) and (22) indicate that the best-estimate predicted value L^{be} of the leakage response will fall in between the initially measured value, L^e, and the computed value, $E\left(L^c\right)$, of the leakage response.

The predicted variance, $\operatorname{var}\left(L^{be}\right)$, of the best-estimate (leakage) response L^{be} is given by the following particular form of the expression derived in [1]:

$$\begin{aligned}\operatorname{var}\left(L^{be}\right) &= \operatorname{var}\left(L^e\right)\left\{1 - \operatorname{var}\left(L^e\right)\left[\operatorname{var}\left(L^e\right) + \operatorname{var}\left(L^c\right)\right]^{-1}\right\} \\ &= \frac{\operatorname{var}\left(L^e\right)\operatorname{var}\left(L^c\right)}{\operatorname{var}\left(L^e\right) + \operatorname{var}\left(L^c\right)}.\end{aligned} \quad (23)$$

Note that the expression in Equation (23) ensures the reduction of the predicted variance $\operatorname{var}\left(L^{be}\right)$ by comparison to either the variance $\operatorname{var}\left(L^e\right)$ of the experimentally measured response or the variance $\operatorname{var}\left(L^c\right)$ of the computed response, since Equation (23) implies the following inequalities:

$$\operatorname{var}\left(L^{be}\right) < \operatorname{var}\left(L^e\right); \quad \operatorname{var}\left(L^{be}\right) < \operatorname{var}\left(L^c\right). \quad (24)$$

The first-order partial sensitivities $\partial L\left(\boldsymbol{\alpha}^0\right)/\partial \alpha_j$, for all α_j, $j = 1, \cdots, TP$, have the following expressions [10]:

$$\frac{\partial L\left(\boldsymbol{\alpha}^0\right)}{\partial q_j} = \sum_{g=1}^{G}\int_0^{r_d} 4\pi r^2 \mathrm{d}r \int_{4\pi} \mathrm{d}\boldsymbol{\Omega}\, \psi^{(1),g}\left(r,\boldsymbol{\Omega}\right)\frac{\partial Q^g\left(\boldsymbol{\alpha}^0\right)}{\partial q_j}, \quad j = 1, \cdots, JQ = 10; \quad (25)$$

$$\begin{aligned}\frac{\partial L\left(\boldsymbol{\alpha}^0\right)}{\partial N_j} &= \sum_{g=1}^{G}\int_0^{r_d} 4\pi r^2 \mathrm{d}r \int_{4\pi} \mathrm{d}\boldsymbol{\Omega}\, \psi^{(1),g}\left(r,\boldsymbol{\Omega}\right)\frac{\partial \Sigma_t^g\left(\boldsymbol{\alpha}^0\right)}{\partial N_j}\varphi^g\left(r,\boldsymbol{\Omega}\right) \\ &- \sum_{h=1}^{G}\int_0^{r_d} 4\pi r^2 \mathrm{d}r \int_{4\pi} \mathrm{d}\boldsymbol{\Omega}'\varphi^h\left(r,\boldsymbol{\Omega}'\right)\left\{\frac{\partial \Sigma_s^{h\to g}\left(\boldsymbol{\alpha}^0;\boldsymbol{\Omega}'\to\boldsymbol{\Omega}\right)}{\partial N_j} + \left\{\frac{\partial\left[\chi^g\left(\nu\Sigma_f\right)^h\right]}{\partial N_j}\right\}_{\boldsymbol{\alpha}^0}\right\},\end{aligned} \quad (26)$$

for $j = 1, \cdots, I = 6$;

$$\frac{\partial L(\boldsymbol{\alpha}^0)}{\partial s_j} = \sum_{g=1}^{G}\int_0^{r_d} 4\pi r^2 \mathrm{d}r \int_{4\pi} \mathrm{d}\boldsymbol{\Omega}\, \psi^{(1),g}(r,\boldsymbol{\Omega})$$
$$\times \sum_{h=1}^{G}\int_0^{r_d} 4\pi r^2 \mathrm{d}r \int_{4\pi} \mathrm{d}\boldsymbol{\Omega}' \frac{\partial \Sigma_s^{h\to g}(\boldsymbol{\alpha}^0;\boldsymbol{\Omega}'\to\boldsymbol{\Omega})}{\partial s_j} \varphi^h(r,\boldsymbol{\Omega}'), \tag{27}$$
$$\text{for } j = 1,\cdots,JSX = (G\times G)\times I\times(ISCT+1) = 21600;$$

$$\frac{\partial L(\boldsymbol{\alpha}^0)}{\partial t_j} = -\sum_{g=1}^{G}\int_0^{r_d} 4\pi r^2 \mathrm{d}r \int_{4\pi} \mathrm{d}\boldsymbol{\Omega}\, \psi^{(1),g}(\boldsymbol{r},\boldsymbol{\Omega})\varphi^g(\boldsymbol{r},\boldsymbol{\Omega}) \frac{\partial \Sigma_t^g(\boldsymbol{\alpha}^0)}{\partial t_j}, \tag{28}$$
$$\text{for } j = 1,\cdots,JTX = 180;$$

$$\frac{\partial L(\boldsymbol{\alpha}^0)}{\partial f_j} = \sum_{g=1}^{G}\int_0^{r_d} 4\pi r^2 \mathrm{d}r \int_{4\pi} \mathrm{d}\boldsymbol{\Omega}\, \psi^{(1),g}(r,\boldsymbol{\Omega})\chi^g(\boldsymbol{\alpha}^0) \sum_{h=1}^{G}\int_0^{r_d} 4\pi r^2 \mathrm{d}r \int_{4\pi} \mathrm{d}\boldsymbol{\Omega}'$$
$$\times \left\{ \frac{\partial\left[(\nu\Sigma_f)^h\right]}{\partial f_j} \right\}_{\boldsymbol{\alpha}^0} \varphi^h(r,\boldsymbol{\Omega}'), \quad \text{for } j = 1,\cdots,JFX = 60; \tag{29}$$

$$\frac{\partial L(\boldsymbol{\alpha}^0)}{\partial \nu_j} = \sum_{g=1}^{G}\int_0^{r_d} 4\pi r^2 \mathrm{d}r \int_{4\pi} \mathrm{d}\boldsymbol{\Omega}\, \psi^{(1),g}(r,\boldsymbol{\Omega})\chi^g(\boldsymbol{\alpha}^0) \sum_{h=1}^{G}\int_0^{r_d} 4\pi r^2 \mathrm{d}r \int_{4\pi} \mathrm{d}\boldsymbol{\Omega}'$$
$$\times \left\{ \frac{\partial\left[(\nu\Sigma_f)^h\right]}{\partial \nu_j} \right\}_{\boldsymbol{\alpha}^0} \varphi^h(r,\boldsymbol{\Omega}'), \quad \text{for } j = 1,\cdots,JNU = 60; \tag{30}$$

$$\frac{\partial L(\boldsymbol{\alpha}^0)}{\partial p_j} = \sum_{g=1}^{G}\int_0^{r_d} 4\pi r^2 \mathrm{d}r \int_{4\pi} \mathrm{d}\boldsymbol{\Omega}\, \psi^{(1),g}(r,\boldsymbol{\Omega}) \frac{\partial \chi^g(\boldsymbol{\alpha}^0)}{\partial p_j}$$
$$\times \sum_{h=1}^{G}\int_0^{r_d} 4\pi r^2 \mathrm{d}r \int_{4\pi} \mathrm{d}\boldsymbol{\Omega}' \left\{(\nu\Sigma_f)^h\right\}_{\boldsymbol{\alpha}^0} \varphi^h(r,\boldsymbol{\Omega}'), \text{ for } j = 1,\cdots,J\chi = 60. \tag{31}$$

In Equations (25)-(31), the 1st-level adjoint function $\boldsymbol{\psi}^{(1)}$ is the solution of the following 1st-Level Adjoint Sensitivity System (1st-LASS):

$$\boldsymbol{A}(\boldsymbol{\alpha})\boldsymbol{\psi}^{(1)}(r,\boldsymbol{\Omega}) = \boldsymbol{I}\left[\boldsymbol{\Omega}\cdot\boldsymbol{n}\delta(r-r_d)\right];\ \boldsymbol{I} \triangleq [1,\cdots,1,\cdots,1]^\dagger, \tag{32}$$

$$\boldsymbol{\psi}^{(1)}(r,\boldsymbol{\Omega}) = \boldsymbol{0},\ r = r_d,\ \boldsymbol{\Omega}\cdot\boldsymbol{n} > 0, \tag{33}$$

where $\boldsymbol{A}(\boldsymbol{\alpha})$ denotes the operator adjoint to $\boldsymbol{B}(\boldsymbol{\alpha})$, having components $A_{gh}(\boldsymbol{\alpha}) \triangleq \left[B_{hg}(\boldsymbol{\alpha})\right]^*$, where the symbol $[\ ]^*$ indicates "formal adjoint operator." In component form, Equations (32) and (33) are as follows:

$$-\boldsymbol{\Omega}\cdot\nabla\psi^{(1),g}(r,\boldsymbol{\Omega}) + \Sigma_t^g(\boldsymbol{\alpha})\psi^{(1),g}(r,\boldsymbol{\Omega}) - \sum_{h=1}^{G}\int_{4\pi} \mathrm{d}\boldsymbol{\Omega}'\psi^{(1),h}(r,\boldsymbol{\Omega}')$$
$$\times\left[\Sigma_s^{g\to h}(\boldsymbol{\alpha};\boldsymbol{\Omega}\to\boldsymbol{\Omega}') + (\nu\Sigma_f)^g(\boldsymbol{\alpha})\chi^h(\boldsymbol{\alpha})\right] = \boldsymbol{\Omega}\cdot\boldsymbol{n}\delta(r-r_d),\ \ g = 1,\cdots,G; \tag{34}$$

$$\psi^{(1),g}(r,\boldsymbol{\Omega}) = 0,\ r = r_d,\ \boldsymbol{\Omega}\cdot\boldsymbol{n} > 0,\ \ g = 1,\cdots,G. \tag{35}$$

The expressions of the sensitivities provided in Equations (25)-(31) are to be evaluated at the nominal values $\boldsymbol{u}^0 \triangleq (\boldsymbol{\varphi}^0;\boldsymbol{\alpha}^0)$. Evidently, the computations of these sensitivities are inexpensive, involving only integrations using quadrature formulas after having obtained the 1st-level adjoint function $\boldsymbol{\psi}^{(1)}(r,\boldsymbol{\Omega})$. The

1st-LASS is independent of parameter variations, so it needs to be solved just once to obtain $\boldsymbol{\psi}^{(1)}(r,\boldsymbol{\Omega})$. Thus, the computation of the TP partial sensitivities $\partial L(\boldsymbol{\alpha}^0)/\partial\alpha_j$, $j=1,\cdots,TP$, requires just a single large-scale computation in order to determine $\boldsymbol{\psi}^{(1)}(r,\boldsymbol{\Omega})$, followed by TP inexpensive computations to perform each integration (quadrature) involving the 1st-level adjoint function $\boldsymbol{\psi}^{(1)}(r,\boldsymbol{\Omega})$.

Each of the first-order sensitivities provided in Equations (25)-(31) gives rise to corresponding 2nd-order sensitivities, which are computed using a 2nd-level adjoint function that is obtained by solving a corresponding 2nd-Level Adjoint Sensitivity System (2nd-LASS). For example, the 2nd-order sensitivities which arise from the 1st-order sensitivities of the response to the total cross sections, cf. Equation (28), have the following expression [10]:

$$\begin{aligned}\sum_{j_2=1}^{TP}\left\{\frac{\partial^2 L(\boldsymbol{\alpha})}{\partial\alpha_{j_2}\partial t_{j_1}}\delta\alpha_{j2}\right\}_{\boldsymbol{\alpha}^0} &= \left\{\sum_{g=1}^{G}\int_0^{r_d}4\pi r^2\mathrm{d}r\int_{4\pi}\mathrm{d}\boldsymbol{\Omega}\psi_1^{(2),g}(j_1;r,\boldsymbol{\Omega})Q^{(1)}(g;\boldsymbol{\alpha},\boldsymbol{\varphi};\delta\boldsymbol{\alpha})\right\}_{\boldsymbol{\alpha}^0}\\ &+\left\{\sum_{g=1}^{G}\int_0^{r_d}4\pi r^2\mathrm{d}r\int_{4\pi}\mathrm{d}\boldsymbol{\Omega}\psi_2^{(2),g}(j_1;r,\boldsymbol{\Omega})Q^{(2)}\left(g;\boldsymbol{\alpha},\boldsymbol{\psi}^{(1)};\delta\boldsymbol{\alpha}\right)\right\}_{\boldsymbol{\alpha}^0},\quad j_1=1,\cdots,JTX.\end{aligned}\tag{36}$$

The 2nd-level adjoint function $\boldsymbol{\psi}^{(2)}(j_1;r,\boldsymbol{\Omega})\triangleq\left[\boldsymbol{\psi}_1^{(2)}(j_1;r,\boldsymbol{\Omega}),\boldsymbol{\psi}_2^{(2)}(j_1;r,\boldsymbol{\Omega})\right]^\dagger$, $\boldsymbol{\psi}_i^{(2)}\triangleq\left(\psi_i^{(2),1},\cdots,u_i^{(2),G}\right)^\dagger$, $i=1,2$, is the solution of the following 2nd-Level Adjoint Sensitivity System (2nd-LASS):

$$\begin{aligned}&\left\{\boldsymbol{A}(\boldsymbol{\alpha})\boldsymbol{\psi}_1^{(2)}(j_1;r,\boldsymbol{\Omega})\right\}_{\boldsymbol{\alpha}^0}\\ &=-\left\{\boldsymbol{S}(j_1;\boldsymbol{\alpha})\boldsymbol{\psi}^{(1)}(r,\boldsymbol{\Omega})\right\}_{\boldsymbol{\alpha}^0},\quad j_1=1,\cdots,JTX=G\times I=180,\end{aligned}\tag{37}$$

$$\left\{\boldsymbol{B}(\boldsymbol{\alpha})\boldsymbol{\psi}_2^{(2)}(j_1;r,\boldsymbol{\Omega})\right\}_{\boldsymbol{\alpha}^0}=-\left\{\boldsymbol{S}(j_1;\boldsymbol{\alpha})\boldsymbol{\varphi}(r,\boldsymbol{\Omega})\right\}_{\boldsymbol{\alpha}^0};\ j_1=1,\cdots,JTX,\tag{38}$$

$$\boldsymbol{\psi}_1^{(2)}(j_1;r,\boldsymbol{\Omega})=\boldsymbol{0},\ r=r_d,\ \boldsymbol{\Omega}\cdot\boldsymbol{n}>0;\ j_1=1,\cdots,JTX,\tag{39}$$

$$\boldsymbol{\psi}_2^{(2)}(j_1;r,\boldsymbol{\Omega})=\boldsymbol{0},\ r=r_d,\ \boldsymbol{\Omega}\cdot\boldsymbol{n}<0;\ j_1=1,\cdots,JTX,\tag{40}$$

where, for each $j_1=1,\cdots,JTX=G\times I=30\times 6=180$, $\boldsymbol{S}(j_1;\boldsymbol{\alpha})$ is a $G\times G$ diagonal matrix having non-zero elements of the form $\partial\Sigma_t^g(\boldsymbol{\alpha})/\partial t_{j_1}$, $g=1,\cdots,G$ on its diagonal, *i.e.*,

$$\boldsymbol{S}(j_1;\boldsymbol{\alpha})\triangleq\begin{pmatrix}\partial\Sigma_t^1(\boldsymbol{\alpha})/\partial t_{j_1} & \bullet & 0\\ \bullet & \bullet & \bullet\\ 0 & \bullet & \partial\Sigma_t^G(\boldsymbol{\alpha})/\partial t_{j_1}\end{pmatrix},\tag{41}$$

$$\begin{aligned}\boldsymbol{Q}^{(1)}(\boldsymbol{\alpha};\delta\boldsymbol{\alpha})&\triangleq\begin{pmatrix}Q^{(1)}\left(1;\boldsymbol{\alpha},\boldsymbol{\psi}^{(1)};\delta\boldsymbol{\alpha}\right)\\ \bullet\\ Q^{(1)}\left(G;\boldsymbol{\alpha},\boldsymbol{\psi}^{(1)};\delta\boldsymbol{\alpha}\right)\end{pmatrix},\\ \boldsymbol{Q}^{(2)}\left(\boldsymbol{\alpha},\boldsymbol{\psi}^{(1)};\delta\boldsymbol{\alpha}\right)&\triangleq\begin{pmatrix}Q^{(2)}\left(1;\boldsymbol{\alpha},\boldsymbol{\psi}^{(1)};\delta\boldsymbol{\alpha}\right)\\ \bullet\\ Q^{(2)}\left(G;\boldsymbol{\alpha},\boldsymbol{\psi}^{(1)};\delta\boldsymbol{\alpha}\right)\end{pmatrix},\end{aligned}\tag{42}$$

$$Q^{(1)}\left(g;\boldsymbol{\alpha},\boldsymbol{\varphi};\delta\boldsymbol{\alpha}\right)\triangleq\frac{\partial Q^{g}\left(\boldsymbol{\alpha}\right)}{\partial\boldsymbol{\alpha}}\delta\boldsymbol{\alpha}-\varphi^{g}\left(r,\boldsymbol{\Omega}\right)\frac{\partial\Sigma_{t}^{g}\left(\boldsymbol{\alpha}\right)}{\partial\boldsymbol{\alpha}}\delta\boldsymbol{\alpha}$$
$$+\sum_{h=1}^{G}\int_{4\pi}\mathrm{d}\boldsymbol{\Omega}'\varphi^{h}\left(r,\boldsymbol{\Omega}'\right)\left\{\frac{\partial\Sigma_{s}^{h\to g}\left(\boldsymbol{\alpha};\boldsymbol{\Omega}'\to\boldsymbol{\Omega}\right)}{\partial\boldsymbol{\alpha}}\delta\boldsymbol{\alpha}+\frac{\partial\left[\chi^{g}\left(\boldsymbol{\alpha}\right)\left(\nu\Sigma_{f}\right)^{h}\left(\boldsymbol{\alpha}\right)\right]}{\partial\boldsymbol{\alpha}}\delta\boldsymbol{\alpha}\right\},\tag{43}$$

$$Q^{(2)}\left(g;\boldsymbol{\alpha},\psi^{(1)};\delta\boldsymbol{\alpha}\right)\triangleq-\psi^{(1),g}\left(r,\boldsymbol{\Omega}\right)\frac{\partial\Sigma_{t}^{g}\left(\boldsymbol{\alpha};r\right)}{\partial\boldsymbol{\alpha}}\delta\boldsymbol{\alpha}$$
$$+\sum_{h=1}^{G}\int_{4\pi}\mathrm{d}\boldsymbol{\Omega}'\psi^{(1),h}\left(r,\boldsymbol{\Omega}'\right)\left\{\frac{\partial\Sigma_{s}^{g\to h}\left(\boldsymbol{\alpha};\boldsymbol{\Omega}\to\boldsymbol{\Omega}'\right)}{\partial\boldsymbol{\alpha}}\delta\boldsymbol{\alpha}+\frac{\partial\left[\left(\nu\Sigma_{f}\right)^{g}\left(\boldsymbol{\alpha}\right)\chi^{h}\left(\boldsymbol{\alpha}\right)\right]}{\partial\boldsymbol{\alpha}}\delta\boldsymbol{\alpha}\right\}.\tag{44}$$

The expressions of the 3rd- and 4th-order sensitivities will not be reproduced here but can be found in [10] [12] [13].

3. Results

This Section presents results that will illustrate the reduction of the predicted standard deviation of the leakage response when applying the 2nd-BERRU-PMD methodology to incorporate a measurement, even when the measurement appears initially to be inconsistent with the computation. The effects of the measurement's precision are also investigated, as are the respective impacts of the 1st-, 2nd-, 3rd- and 4th-order sensitivities. Results are also presented for illustrating the effects of parameters standard deviations which are within, borderline, or outside of the radius of convergence of the Taylor-series provided in Equation (17).

3.1. High-Precision Measured Response ($L^{e}=3.0\times10^{6}$ Neutrons/Sec; Relative $SD^{(e)}=2\%$) and High Precision Parameters (Relative SD = 3%)

This section presents the results produced by using the 2nd-BERRU-PMD in conjunction with an experimental response measured with high precision, and models parameters which are also known fairly precisely, all having relative standard deviations of 3%. For uniform relative standard deviations of 3% for the model parameters, the approximate radius of convergence for the Taylor-series presented in Equation (17) can be computed by considering the convergence "ratio-test." The ratio of the 3rd-order term with respect to the 2nd-order term of the Taylor series is 0.58; and the ratio of the 4th-order term with respect to the 3rd-order term of the Taylor series is 0.68. Both of these results are well below 1.00, which indicates that the Taylor-series is expected to be convergent for unform relative standard deviations of 3% for the model parameters.

3.1.1. Including Only Contributions from the 1st-Order Sensitivities of the Leakage Response to the Total Cross Sections

Almost all of the largest sensitivities (1st-through 4th-order) of the leakage response are with respect to the total cross sections. When only the 1st-order sensi-

tivities with respect to the total cross sections are considered, the 2nd-BERRU-PMD expressions shown in Equations (20) and (23), respectively, yield the results presented in Table 3 and depicted in Figure 2, below.

The results presented in Table 3 and Figure 2 indicate that:

1) The inequality $E\left(L^c\right) < L^{be} < L^e$, predicted by Equation (22), is fulfilled, as expected.

2) The reduction of the predicted standard deviation of the predicted response, predicted by Equation (24), has been accomplished; the numerical results given in Table 3 indicate that $SD^{(be,1)} < SD^{(e)} < SD^{(1)}$.

3) However, the computed results, which only include the contributions stemming from the 1st-order sensitivities, appear to be inconsistent with the experimental results. This apparent inconsistency occurs despite the fact that the Taylor-series in Equation (17) is expected to be convergent. Thus, this apparent "inconsistency between computation and experiment" indicates that, at the very least, the contributions stemming from the 2nd-order sensitivities must also be included.

The results obtained by including the contributions from both the 1st-order and 2nd-order sensitivities are presented in Subsection 3.1.2, below.

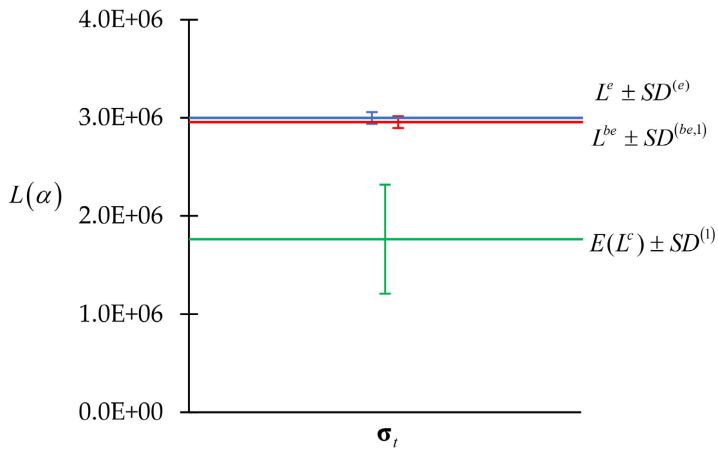

Figure 2. Comparison of $E\left(L^c\right) \pm SD^{(1)}$ (in green), $L^{be} \pm SD^{(be,1)}$ (in red), $L^e \pm SD^{(e)}$ (in blue), due to 3% standard deviations for uncorrelated and normally distributed total microscopic cross sections σ_t, when only the first-order sensitivities are considered.

Table 3. Values of $E\left(L^c\right) \pm SD^{(1)}$, $L^{be} \pm SD^{(be,1)}$, $L^e \pm SD^{(e)}$, due to 3% standard deviations for uncorrelated and normally distributed total microscopic cross sections σ_t, when only the first-order sensitivities are considered.

Responses	Numerical Values (only σ_t)
$E\left(L^c\right) \pm SD^{(1)}$	$1.765 \times 10^6 \pm 5.548 \times 10^5$
$L^{be} \pm SD^{(be,1)}$	$2.956 \times 10^6 \pm 5.965 \times 10^4$
$L^e \pm SD^{(e)}$	$3.000 \times 10^6 \pm 6.000 \times 10^4$

3.1.2. Including Contributions from the 1st + 2nd -Order Sensitivities of the Leakage Response to the Total Cross Sections

The numerical results obtained by including in Equations (20) and (23) the contributions stemming from the 1st + 2nd-order sensitivities of the leakage response to the total cross sections are presented in Table 4 and depicted in Figure 3, below.

The results presented in Table 4 and Figure 3 indicate that:

1) The inequality $E\left(L^c\right) < L^{be} < L^e$ predicted by Equation (22) is fulfilled, as expected.

2) The expected value $E\left(L^c\right)$ of the computed response approaches from below the values of both the best estimate value L^{be} and the experimentally measured mean/nominal value L^e.

3) The inequality $SD^{(be,2)} < SD^{(e)} < SD^{(2)}$, predicted by Equation (24), is preserved. By comparison to the results shown in Table 3, the inclusion of the contributions stemming from the 2nd-order sensitivities (in addition to the contributions stemming from the 1st-order sensitivities) brings the best-estimate predicted value L^{be} closer to the precisely-measured value L^e.

4) However, the "computed results" for the response are still slightly inconsistent with the "experimental results." This inconsistency, albeit small, indicates

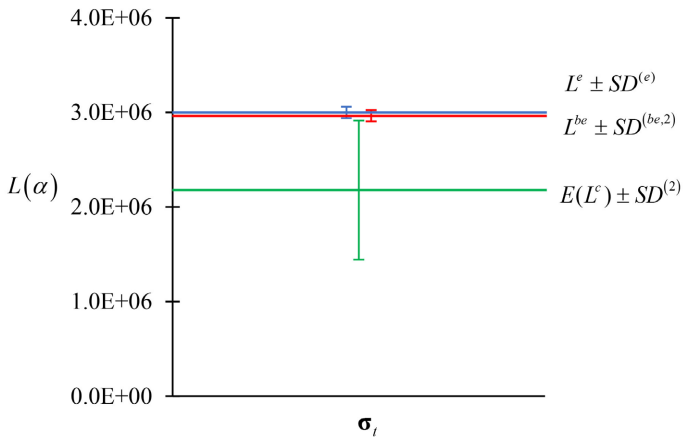

Figure 3. Comparison of $E\left(L^c\right) \pm SD^{(2)}$ (in green), $L^{be} \pm SD^{(be,2)}$ (in red), $L^e \pm SD^{(e)}$ (in blue), due to 3% standard deviations for uncorrelated and normally distributed total microscopic cross sections σ_t, when the 1st + 2nd-order sensitivities are included.

Table 4. Values of $E\left(L^c\right) \pm SD^{(2)}$, $L^{be} \pm SD^{(be,2)}$, $L^e \pm SD^{(e)}$, due to 3% standard deviations for uncorrelated and normally distributed total microscopic cross sections σ_t, when the 1st + 2nd-order sensitivities are included.

Responses	Numerical Values (only σ_t)
$E\left(L^c\right) \pm SD^{(2)}$	$2.179 \times 10^6 \pm 7.355 \times 10^5$
$L^{be} \pm SD^{(be,2)}$	$2.995 \times 10^6 \pm 5.980 \times 10^4$
$L^e \pm SD^{(e)}$	$3.000 \times 10^6 \pm 6.000 \times 10^4$

that the contributions from the 3rd-order sensitivities must also be included, in addition to the contributions stemming from the 1st-order and the 2nd-order sensitivities.

The results obtained by including the contributions from the 1st-, 2nd-, and 3rd-order sensitivities are presented in Subsection 3.1.3, below.

3.1.3. Including Contributions from the 1st + 2nd + 3rd-Order Sensitivities of the Leakage Response to the Total Cross Sections

The numerical results obtained by including in Equations (20) and (23) the contributions stemming from the 1st + 2nd + 3rd-order sensitivities of the leakage response to the total cross sections are presented in Table 5 and depicted in Figure 4, below.

The results presented in Table 5 and Figure 4 indicate that:

1) The inequality $E\left(L^c\right) < L^{be} < L^e$ predicted by Equation (22) is fulfilled, as expected.

2) The expected value $E\left(L^c\right)$ of the computed response continues to approach monotonically from below the values of both the best estimate value L^{be} and the experimentally measured mean/nominal value L^e.

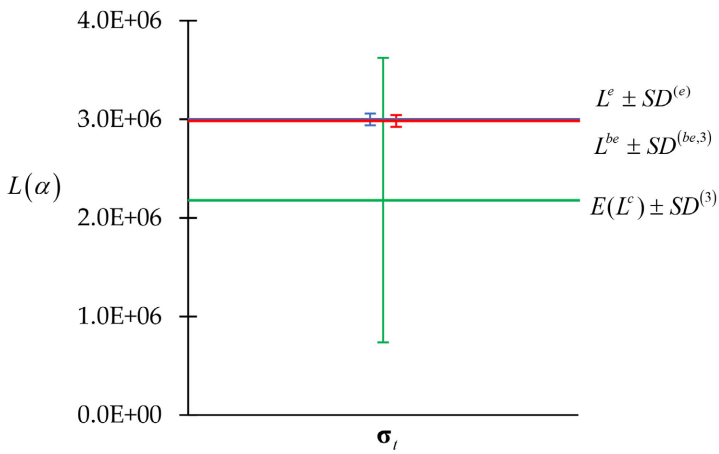

Figure 4. Comparison of $E\left(L^c\right) \pm SD^{(3)}$ (in green), $L^{be} \pm SD^{(be,3)}$ (in red), $L^e \pm SD^{(e)}$ (in blue), due to 3% standard deviations for uncorrelated and normally distributed total microscopic cross sections σ_t, when the 1st + 2nd + 3rd-order sensitivities are included.

Table 5. Values of $E\left(L^c\right) \pm SD^{(3)}$, $L^{be} \pm SD^{(3)}$, $L^e \pm SD^{(e)}$, due to 3% standard deviations for uncorrelated and normally distributed total microscopic cross sections σ_t, when the 1st + 2nd + 3rd-order sensitivities are included.

Responses	Numerical Values (only σ_t)
$E\left(L^c\right) \pm SD^{(3)}$	$2.179 \times 10^6 \pm 1.443 \times 10^6$
$L^{be} \pm SD^{(3)}$	$2.999 \times 10^6 \pm 5.995 \times 10^4$
$L^e \pm SD^{(e)}$	$3.000 \times 10^6 \pm 6.000 \times 10^4$

3) The inequality $SD^{(be,3)} < SD^{(e)} < SD^{(3)}$, predicted by Equation (24), is preserved. By comparison to the results shown in Table 4, the inclusion of the contributions stemming from the 3rd-order sensitivities (in addition to the contributions stemming from the 1st- and 2nd-order sensitivities) brings the best-estimate predicted value L^{be} even closer to the precisely-measured value L^{e}.

4) The "computed results" for the response are now consistent with the "experimental results."

The results obtained by including the contributions from the 1st-, 2nd-, 3rd-, and 4th-order sensitivities are presented in Subsection 3.1.4, below.

3.1.4. Including Contributions from the 1st + 2nd + 3rd + 4th-Order Sensitivities of the Leakage Response to the Total Cross Sections

The numerical results obtained by including in Equations (20) and (23) the contributions stemming from the 1st + 2nd + 3rd + 4th-order sensitivities of the leakage response to the total cross sections are presented in Table 6 and depicted in Figure 5, below.

The results presented in Table 6 and Figure 5 indicate that:

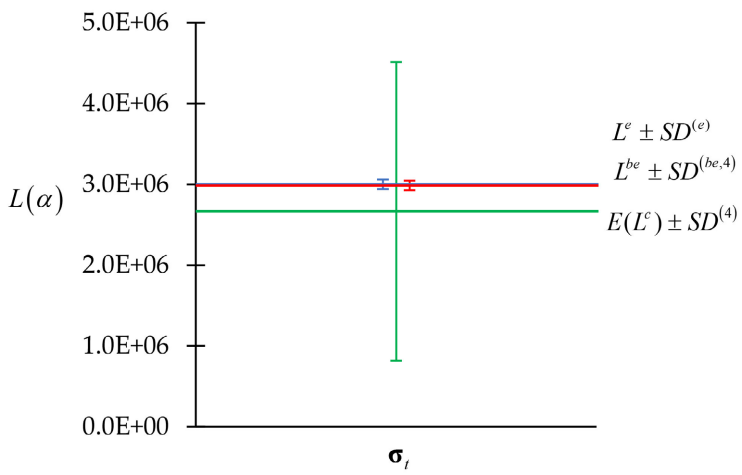

Figure 5. Comparison of $E(L^c) \pm SD^{(4)}$ (in green), $L^{be} \pm SD^{(be,4)}$ (in red), $L^{e} \pm SD^{(e)}$ (in blue), due to 3% standard deviations for uncorrelated and normally distributed total microscopic cross sections σ_t, when the 1st + 2nd + 3rd + 4th-order sensitivities are included.

Table 6. Values of $E(L^c) \pm SD^{(4)}$, $L^{be} \pm SD^{(be,4)}$, $L^{e} \pm SD^{(e)}$, due to 3% standard deviations for uncorrelated and normally distributed total microscopic cross sections σ_t, when the 1st + 2nd + 3rd + 4th-order sensitivities are included.

Responses	Numerical Values (only σ_t)
$E(L^c) \pm SD^{(4)}$	$2.667 \times 10^6 \pm 1.847 \times 10^6$
$L^{be} \pm SD^{(be,4)}$	$2.999 \times 10^6 \pm 5.997 \times 10^4$
$L^{e} \pm SD^{(e)}$	$3.000 \times 10^6 \pm 6.000 \times 10^4$

1) The inequality $E\left(L^c\right) < L^{be} < L^e$ predicted by Equation (22) is fulfilled, as expected.

2) The expected value $E\left(L^c\right)$ of the computed response continued to approach monotonically from below the values of both the best estimate value L^{be} and the experimentally measured mean/nominal value L^e.

3) The inequality $SD^{(be,4)} < SD^{(e)} < SD^{(4)}$, predicted by Equation (24), is preserved. By comparison to the results shown in Table 4, the inclusion of the contributions stemming from the 4th-order sensitivities (in addition to the contributions stemming from the 1st - 2nd- and 3rd-order sensitivities) practically renders the best-estimate predicted value L^{be} to be the same as the precisely-measured value L^e.

4) The "computed results" for the response are consistent with the "experimental results."

The additional contributions from the 4th-order sensitivities have only insignificantly changed the results obtained by having included only the sensitivities up to 3rd-order. This conclusion indicates that it is not necessary to include contributions from 5th- and higher-order, since their contributions are expected to be increasingly less significant as their order increases, because the Taylor-series provided in Equation (17) is convergent for the parameter standard deviations (3%) considered in this illustrative example.

3.2. High-Precision Measured Response ($L^e = 3.0\times10^6$ Neutrons/Sec; Relative $SD^{(e)} = 2\%$) and Low Precision Parameters (Relative SD = 10%, Outside of Taylor-Series Convergence Radius)

This section presents the results produced by using the 2nd-BERRU-PMD in conjunction with an experimental response measured with high precision, but with rather imprecisely known model parameters, all having relative standard deviations of 10%. Such standard deviations are not prevalent in practice but may nevertheless be encountered for total cross sections. The ratio of the 3rd-order term with respect to the 2nd-order term of the Taylor series is 1.93; the ratio of the 4th-order term with respect to the 3rd-order term of the Taylor series is 2.26. Both of these results are larger than 1.00, which indicates that the Taylor-series presented in Equation (17) is being used outside its radius of convergence to compute the response's expected value and variance. This illustrative example involving precise measurements, but rather imprecise parameters has been deliberately chosen in order to underscore the decisive impact of higher-order sensitivities and the ability of the 2nd-BERRU-PMD methodology to yield best-estimate results with reduced uncertainties despite the imprecisely known model parameters.

3.2.1. Including Only Contributions from the 1st-Order Sensitivities of the Leakage Response to the Total Cross Sections

When only the 1st-order sensitivities with respect to the total cross sections are

considered, the 2nd-BERRU-PMD expressions shown in Equations (20) and (23), respectively, yield the results presented in Table 7 and depicted in Figure 6, below.

The results presented in Table 7 and Figure 6 indicate that:

1) The inequality $E\left(L^c\right) < L^{be} < L^e$, predicted by Equation (22), is fulfilled, as expected; the best-estimate response value L^{be} practically coincides with the nominal value L^e of the experimental response.

2) The reduction of the predicted standard deviation of the predicted response, predicted by Equation (24), has been accomplished; the numerical results given in Table 7 indicate that $SD^{(be,1)} < SD^{(e)} < SD^{(1)}$; $SD^{(e)} \cong SD^{(be,1)}$.

3) The computed results are consistent with the experimental results, even though only the contributions stemming from the 1st-order sensitivities are included. This apparent consistency occurs despite the fact that the Taylor-series in Equation (17) is expected to be divergent for the value of 10% considered (uniformly) for the relative standard deviations of parameters.

The results obtained by including the contributions from both the 1st-order and 2nd-order sensitivities are presented in Subsection 3.2.2, below.

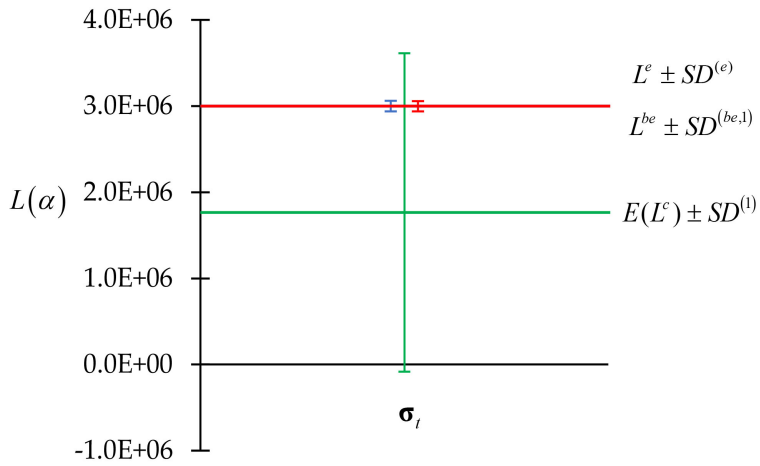

Figure 6. Comparison of $E\left(L^c\right) \pm SD^{(1)}$ (in green), $L^{be} \pm SD^{(be,1)}$ (in red), $L^e \pm SD^{(e)}$ (in blue), due to 10% standard deviations for uncorrelated and normally distributed total microscopic cross sections σ_t, when only the first-order sensitivities are considered.

Table 7. Values of $E\left(L^c\right) \pm SD^{(1)}$, $L^{be} \pm SD^{(be,1)}$, $L^e \pm SD^{(e)}$, due to 10% standard deviations for uncorrelated and normally distributed total microscopic cross sections σ_t, when only the first-order sensitivities are considered.

Responses	Numerical Values (only σ_t)
$E\left(L^c\right) \pm SD^{(1)}$	$1.765 \times 10^6 \pm 1.849 \times 10^6$
$L^{be} \pm SD^{(be,1)}$	$2.999 \times 10^6 \pm 5.997 \times 10^4$
$L^e \pm SD^{(e)}$	$3.000 \times 10^6 \pm 6.000 \times 10^4$

3.2.2. Including Contributions from the 1st + 2nd-Order Sensitivities of the Leakage Response to the Total Cross Sections

When both the 1st-order and 2nd-order sensitivities with respect to the total cross sections are considered, the 2nd-BERRU-PMD expressions shown in Equations (20) and (23), respectively, yield the results presented in Table 8 and depicted in Figure 7, below.

The results presented in Table 8 and Figure 7 indicate that:

1) The inequality $E\left(L^c\right) < L^{be} < L^e$, predicted by Equation (22), is violated, thus indicating the effects of the divergence of the Taylor-series in Equation (17) for the value of 10% considered for the relative standard deviations of parameters. The best-estimate response value L^{be} practically coincides with the nominal value L^e of the experimental response.

2) The numerical results given in Table 8 indicate that $SD^{(e)} \cong SD^{(be,2)}$.

Comparing the results provided in Table 8 with the results provided in Table 4 indicates that when considering an accurate measurement but inaccurate parameters, the 2nd-BERRU-PMD uses the "flexibility" provided by the inaccurate parameters (as opposed to the constraints stemming from the accurately known parameters considered in Table 4) to yield best-estimate nominal response values

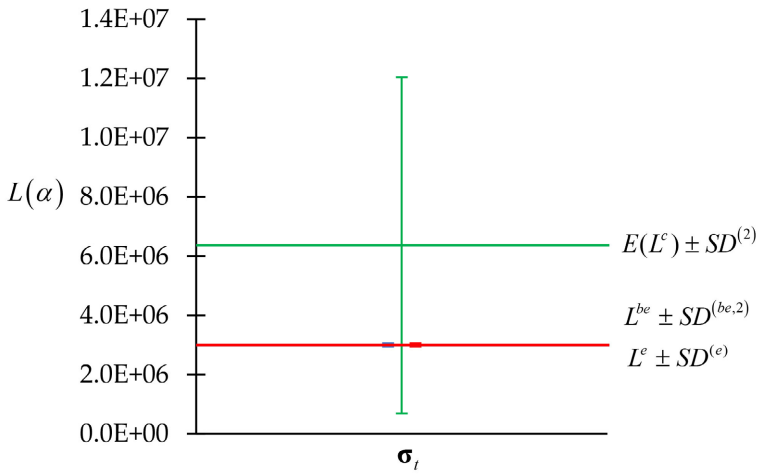

Figure 7. Comparison of $E\left(L^c\right) \pm SD^{(2)}$ (in green), $L^{be} \pm SD^{(be,2)}$ (in red), $L^e \pm SD^{(e)}$ (in blue), due to 10% standard deviations for uncorrelated and normally distributed total microscopic cross sections σ_t, when the 1st + 2nd-order sensitivities are included.

Table 8. Values of $E\left(L^c\right) \pm SD^{(2)}$, $L^{be} \pm SD^{(be,2)}$, $L^e \pm SD^{(e)}$, due to 10% standard deviations for uncorrelated and normally distributed total microscopic cross sections σ_t, when the 1st + 2nd-order sensitivities are included.

Responses	Numerical Values (only σ_t)
$E\left(L^c\right) \pm SD^{(2)}$	$6.363 \times 10^6 \pm 5.675 \times 10^6$
$L^{be} \pm SD^{(be,2)}$	$3.001 \times 10^6 \pm 5.999 \times 10^4$
$L^e \pm SD^{(e)}$	$3.000 \times 10^6 \pm 6.000 \times 10^4$

that practically coincides with the precisely measured response value, while significantly reducing the accompanying predicted best-estimate standard deviations. After including the 2nd-order sensitivities and noting that their inclusion had no practical effects (as can be concluded by intercomparing the results presented in Table 7 and Table 8), it becomes apparent that higher-order sensitivities are not needed; the values of the best-estimate response and accompanying best-estimate standard deviation have been already provided by using just the 1st-order sensitivities (results presented in Table 7), as confirmed by the results presented in Table 8, which imply that even the 2nd-order sensitivities have insignificant impact in the case considered (high precision measurement and imprecisely known model parameters).

3.3. Low-Precision Measured Response ($L^e = 7.0\times10^6$ Neutrons/Sec; Relative $SD^{(e)} = 10\%$); Borderline Parameter Precision (Relative SD = 5%)

This section presents the results produced by using the 2nd-BERRU-PMD in conjunction with an experimental response measured with low precision, and relatively imprecisely known model parameters, all having relative standard deviations of 5%, which often occurs in practice. The ratio of the 3rd-order term with respect to the 2nd-order term of the Taylor series is 0.97 < 1.00, but the ratio of the 4th-order term with respect to the 3rd-order term of the Taylor series is 1.13 > 1.00. These ratios indicate that relative standard deviations of 5% for the model parameters are "borderline" values regarding the convergence (or non-convergence) of the Taylor-series presented in Equation (17). Thus, this illustrative example involves a low-precision measurement and model parameters that are representative of the "usual uncertainties encountered in practice." The has been deliberately chosen in order to underscore the impact of the higher-order response sensitivities to parameters when the parameter uncertainties are representative of uncertainties usually encountered in practice while also being "borderline" in terms of the convergence of the Taylor-series that underlies the determination of the statistics (expected values, variance, etc.) of the distribution of the computed response in the phase-space of imprecisely known model parameters.

3.3.1. Including Only Contributions from the 1st-Order Sensitivities of the Leakage Response to All Important Parameters

Table 9 presents numerical results obtained for the expected value and standard deviation of the computed response, together with the best estimate mean value and best-estimate standard deviation for the best-estimate response, when considering the 1st-order sensitivities with respect to the total cross sections and, in parallel, considering all of the important 1st-order response sensitivities (*i.e.*, with respect to the total cross sections, fission cross section, fission parameters and isotopic atomic densities). The numerical results presented in Table 9 are depicted in Figure 8.

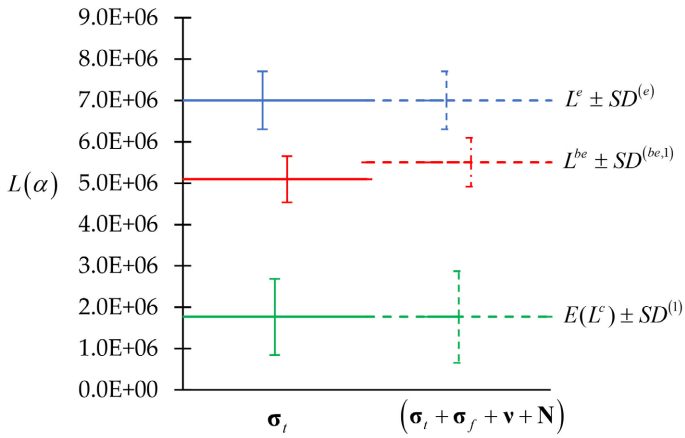

Figure 8. Comparison of $E(L^c) \pm SD^{(1)}$ (in green), $L^{be} \pm SD^{(be,1)}$ (in red), $L^e \pm SD^{(e)}$ (in blue), due to 5% standard deviations for uncorrelated and normally distributed total microscopic cross sections $\boldsymbol{\sigma}_t$, and all important parameters $(\boldsymbol{\sigma}_t + \boldsymbol{\sigma}_f + \boldsymbol{\nu} + \boldsymbol{N})$, when the first-order sensitivities are considered.

Table 9. Values of $E(L^c) \pm SD^{(1)}$, $L^{be} \pm SD^{(be,1)}$, $L^e \pm SD^{(e)}$, due to 5% standard deviations for uncorrelated and normally distributed total microscopic cross sections $\boldsymbol{\sigma}_t$, and all important parameters $(\boldsymbol{\sigma}_t + \boldsymbol{\sigma}_f + \boldsymbol{\nu} + \boldsymbol{N})$, when only the first-order sensitivities are considered.

Responses	Numerical Values For $\boldsymbol{\sigma}_t$	Numerical Values For $(\boldsymbol{\sigma}_t + \boldsymbol{\sigma}_f + \boldsymbol{\nu} + \boldsymbol{N})$
$E(L^c) \pm SD^{(1)}$	$1.765 \times 10^6 \pm 9.246 \times 10^5$	$1.765 \times 10^6 \pm 1.107 \times 10^6$
$L^{be} \pm SD^{(be,1)}$	$5.093 \times 10^6 \pm 5.581 \times 10^5$	$5.505 \times 10^6 \pm 5.916 \times 10^5$
$L^e \pm SD^{(e)}$	$7.000 \times 10^6 \pm 7.000 \times 10^5$	$7.000 \times 10^6 \pm 7.000 \times 10^5$

The results presented in **Table 9** and **Figure 8** indicate that:

1) The inequality $E(L^c) < L^{be} < L^e$, predicted by Equation (22), is fulfilled both when considering only the total cross sections and when considering all of the important model parameters. The predicted response value, L^{be}, is closer to the experimentally measured value when the 1st-order sensitivities to all important parameters are included.

2) The reduction of the predicted standard deviation to a value smaller than either the originally computed or the measured standard deviations, *i.e.*, $SD^{(be,1)} < SD^{(e)}$ and $SD^{(be,1)} < SD^{(1)}$, which is guaranteed by the application of the 2nd-BERRU-PMD methodology, is also apparent.

3) The computed results are apparently inconsistent with the experimental results, both if only the total cross sections and also if all important model parameters are considered.

4) The contributions of the 1st-order sensitivities stemming from the additional parameters (*i.e.*, the parameters in addition to the total cross sections) are in-

significant.

The results obtained by including the contributions from both the 1st-order and 2nd-order sensitivities are presented in Subsection 3.3.2, below.

3.3.2. Including Contributions from the 1st + 2nd-Order Sensitivities of the Leakage Response to All Important Parameters

Table 10 presents numerical results obtained for the expected value and standard deviation of the computed response, together with the best estimate mean value and best-estimate standard deviation for the best-estimate response, when considering the 1st- and 2nd-order sensitivities with respect to the total cross sections. In parallel, Table 10 also presents numerical results obtained for the expected value and standard deviation of the computed response, together with the best estimate mean value and best-estimate standard deviation for the best-estimate response, when considering the 1st- and 2nd-order sensitivities with respect to all of the significant model parameters (total cross sections, fission cross section, fission parameters and isotopic atomic densities). The numerical results presented in Table 10 are depicted in Figure 9.

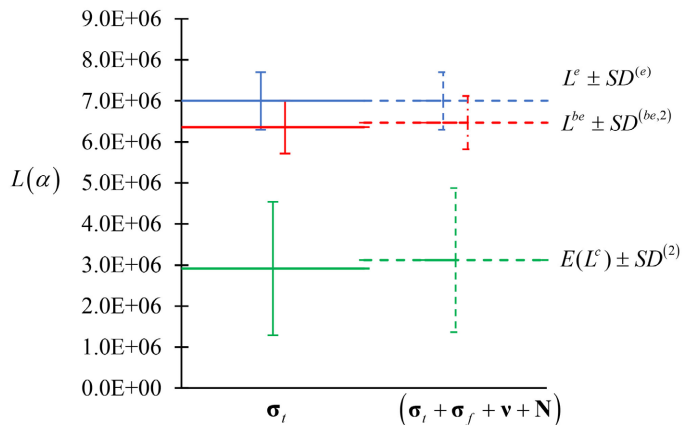

Figure 9. Comparison of $E(L^c) \pm SD^{(2)}$ (in green), $L^{be} \pm SD^{(be,2)}$ (in red), $L^e \pm SD^{(e)}$ (in blue), due to 5% standard deviations of the uncorrelated and normally distributed total microscopic cross sections $\boldsymbol{\sigma}_t$ and all important parameters $(\boldsymbol{\sigma}_t + \boldsymbol{\sigma}_f + \boldsymbol{\nu} + \boldsymbol{N})$, when the 1st + 2nd-order sensitivities are included.

Table 10. Values of $E(L^c) \pm SD^{(2)}$, $L^{be} \pm SD^{(be,2)}$, $L^e \pm SD^{(e)}$, due to 5% standard deviations for uncorrelated total microscopic cross sections $\boldsymbol{\sigma}_t$ and all important parameters $(\boldsymbol{\sigma}_t + \boldsymbol{\sigma}_f + \boldsymbol{\nu} + \boldsymbol{N})$, when the 1st + 2nd-order sensitivities are included.

Responses	Numerical Values For $\boldsymbol{\sigma}_t$	Numerical Values For $(\boldsymbol{\sigma}_t + \boldsymbol{\sigma}_f + \boldsymbol{\nu} + \boldsymbol{N})$
$E(L^c) \pm SD^{(2)}$	$2.914 \times 10^6 \pm 1.629 \times 10^6$	$3.120 \times 10^6 \pm 1.754 \times 10^6$
$L^{be} \pm SD^{(be,2)}$	$6.363 \times 10^6 \pm 6.431 \times 10^5$	$6.467 \times 10^6 \pm 6.502 \times 10^5$
$L^e \pm SD^{(e)}$	$7.000 \times 10^6 \pm 7.000 \times 10^5$	$7.000 \times 10^6 \pm 7.000 \times 10^5$

The results presented in Table 10 and Figure 9 indicate that:

1) The inequality $E\left(L^c\right) < L^{be} < L^e$, predicted by Equation (22), is fulfilled both when considering only the total cross sections and when considering all of the important model parameters. The predicted response value, L^{be}, is closer to the experimentally measured value when the 1st- and 2nd-order sensitivities to all important parameters are included.

2) As guaranteed by the application of the 2nd-BERRU-PMD methodology, the reduction of the predicted standard deviation to a value smaller than either the originally computed or the measured standard deviations, *i.e.*, $SD^{(be,2)} < SD^{(e)}$ and $SD^{(be,2)} < SD^{(2)}$, is apparent.

3) The computed results are apparently still inconsistent (albeit less so than when only the 1st-order sensitivities are included) with the experimental results, both if only the total cross sections and also if all important model parameters are considered.

4) The contributions of the 1st- and 2nd-order sensitivities stemming from the additional parameters (*i.e.*, the parameters in addition to the total cross sections) are insignificant. This observation indicates that the contributions of the higher-order sensitivities stemming from the model parameters other than the total cross sections can be omitted by comparison to the contributions of the higher-order sensitivities stemming just from the total cross sections.

The results obtained by including the contributions from the 1st-, 2nd-, and 3rd-order sensitivities are presented in Subsection 3.3.3, below.

3.3.3. Including Contributions from the 1st + 2nd + 3rd-Order Sensitivities of the Leakage Response to the Total Cross Sections

Table 11 presents numerical results obtained for the expected value and standard deviation of the computed response, together with the best estimate mean value and best-estimate standard deviation for the best-estimate response, when considering the 1st-, 2nd-, and 3rd-order sensitivities with respect to the total cross sections. The numerical results presented in Table 11 are depicted in Figure 10.

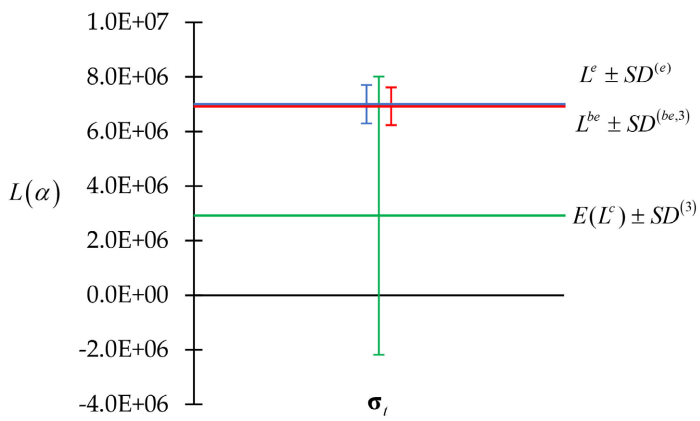

Figure 10. Comparison of $E\left(L^c\right) \pm SD^{(3)}$ (in green), $L^{be} \pm SD^{(be,3)}$ (in red), $L^e \pm SD^{(e)}$ (in blue), due to 5% standard deviations for uncorrelated and normally distributed total microscopic cross sections σ_t, when the 1st + 2nd + 3rd-order sensitivities are included.

Table 11. Values of $E\left(L^c\right) \pm SD^{(3)}$, $L^{be} \pm SD^{(be,3)}$, $L^e \pm SD^{(e)}$, due to 5% standard deviations for uncorrelated and normally distributed total microscopic cross sections σ_t, when the 1st + 2nd + 3rd-order sensitivities are included.

Responses	Numerical Values (only σ_t)
$E\left(L^c\right) \pm SD^{(3)}$	$2.914 \times 10^6 \pm 5.103 \times 10^6$
$L^{be} \pm SD^{(be,3)}$	$6.925 \times 10^6 \pm 6.935 \times 10^5$
$L^e \pm SD^{(e)}$	$7.000 \times 10^6 \pm 7.000 \times 10^5$

The results presented in **Table 11** and **Figure 10** indicate that:

1) The inequality $E\left(L^c\right) < L^{be} < L^e$, predicted by Equation (22), is fulfilled. The predicted response value, L^{be}, is much closer to the experimentally measured value when also including the contributions stemming from the 3rd-order sensitivities (in addition to the contributions stemming from the 1st- and 2nd-order ones).

2) As guaranteed by the application of the 2nd-BERRU-PMD methodology, the reduction of the predicted standard deviation to a value smaller than either the originally computed or the measured standard deviations, *i.e.*, $SD^{(be,3)} < SD^{(e)}$ and $SD^{(be,3)} < SD^{(3)}$, is apparent.

3) When the contributions stemming from the 3rd-order are also included, the computed results become consistent with the experimental results.

The results obtained by including the contributions from the 1st-, 2nd-, 3rd-, and 4th-order sensitivities are presented in Subsection 3.3.4, below.

3.3.4. Including Contributions from the 1st + 2nd + 3rd + 4th-Order Sensitivities of the Leakage Response to the Total Cross Sections

Table 12 presents numerical results obtained for the best estimate mean value and best-estimate standard deviation for the best-estimate response, together with numerical results for the expected value and standard deviation of the computed response, when considering the 1st-, 2nd-, 3rd-, and 4th-order sensitivities with respect to the total cross sections. The numerical results presented in **Table 12** are depicted in **Figure 11**.

The results presented in **Table 12** and **Figure 11** indicate that:

1) The inequality $E\left(L^c\right) < L^{be} < L^e$, predicted by Equation (22), is fulfilled. All three of these quantities have remarkably clustered together, with $L^{be} \cong L^e$.

2) As guaranteed by the application of the 2nd-BERRU-PMD methodology, the reduction of the predicted standard deviation to a value smaller than either the originally computed or the measured standard deviations, *i.e.*, $SD^{(be,4)} < SD^{(e)}$ and $SD^{(be,4)} < SD^{(4)}$, is apparent.

3) Comparing the results presented in **Table 11** with the corresponding results presented in **Table 12** indicates that the 4th-order sensitivities contribute very little to the respective results; in turn, this observation indicates that higher-order sensitivities need not be considered.

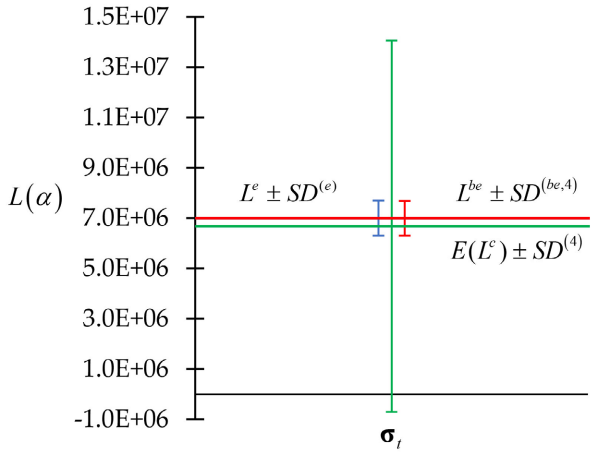

Figure 11. Comparison of $E\left(L^c\right) \pm SD^{(4)}$ (in green), $L^{be} \pm SD^{(be,4)}$ (in red), $L^e \pm SD^{(e)}$ (in blue), due to 5% standard deviations for uncorrelated and normally distributed total microscopic cross sections σ_t, when the 1st + 2nd + 3rd + 4th-order sensitivities are included.

Table 12. Values of $E\left(L^c\right) \pm SD^{(4)}$, $L^{be} \pm SD^{(be,4)}$, $L^e \pm SD^{(e)}$, due to 5% standard deviations for uncorrelated and normally distributed total microscopic cross sections σ_t, when the 1st + 2nd + 3rd + 4th-order sensitivities are included.

Responses	Numerical Values (only σ_t)
$E\left(L^c\right) \pm SD^{(4)}$	$6.681 \times 10^6 \pm 7.386 \times 10^6$
$L^{be} \pm SD^{(be,4)}$	$6.997 \times 10^6 \pm 6.969 \times 10^5$
$L^e \pm SD^{(e)}$	$7.000 \times 10^6 \pm 7.000 \times 10^5$

4. Discussion and Conclusion

Using the maximum entropy (MaxEnt) principle of thermodynamics [3] and concepts of information theory [4], Cacuci [1] [2] has conceived the 2nd-BERRU-PM methodology; this acronym stands for "second-order predictive modelling methodology conceived by for obtaining "best-estimate results with reduced uncertainties." The conceptual underpinnings of the 2nd-BERRU-PM methodology are in contradistinction to the data assimilation methodology [5], which relies on minimizing a subjective user-defined functional which is meant to represent, in the energy-norm, the differences between measured and computed results of interest (called "responses"). The 2nd-BERRU-PM methodology can be constructed either by incorporating the representation of the computational model deterministically (yielding the "2nd-BERRU-PMD" [1] methodology) or by incorporating the representation of the computational model probabilistically (yielding the alternative "2nd-BERRU-PMP" [2] methodology). These methodologies yield equivalent but not identical expression for the predicted results (second-order best-estimate predicted values for the predicted model response and calibrated model parameters, along with reduced predicted best-estimate

standard deviations).

This work has illustrated the application of the 2nd-BERRU-PMD [1] methodology to illustrate quantitatively the effects of second- and higher-order sensitivities for obtaining best-estimate results with reduced uncertainties for the polyethylene-reflected plutonium (acronym: PERP) OECD/NEA reactor physics benchmark [6]. This benchmark is modeled using the neutron transport Boltzmann equation, the solution of which is representative of "large-scale computations" and involves a large number (21,976) of uncertain parameters. Several representative practical situations have been considered, as follows: 1) high-precision measured response and high precision parameters; 2) high-precision measured response and low precision parameters; 3) low-precision measured response and borderline (in terms of convergence of the expressions underlying the computation of the expected value and, respectively, the standard deviation of the computed response) parameter precision. In all situations, as predicted by the 2nd-BERRU-PMD [1] methodology, the predicted best-estimate value of the response has fallen in between the computed and measured values of the leakage response. Also as predicted by the 2nd-BERRU-PMD [1] methodology, it has been observed that the predicted standard deviation of the predicted response is smaller than either the measure or the computed standard deviation, regardless of the order of sensitivities included in the respective computation, *i.e.*, $SD^{(be)} < SD^{(e)}$ and $SD^{(be)} < SD^{(comp)}$. It has also been observed that when the parameters are known with high precision, the contributions of the higher-order sensitivities diminish with increasing order, so that the inclusion of the 2nd-order sensitivities (in addition to the 1st-order sensitivities), while necessary, may suffice for obtaining accurate predicted best-estimate response values and best-estimate standard deviations. On the other hand, when the parameters' standard deviations are sufficiently large to approach (or be outside of) the radius of convergence of the multivariate Taylor-series which represents the response in the phase-space of model parameters, the contributions of the 3rd- and even 4th-order sensitivities are necessary to ensure consistency between the computed and measured response. In such cases, the use of only the 1st-order sensitivities invariably indicates erroneously that the computed results are inconsistent with the respective measured response.

The results presented in this work indicate the general conclusion that at least the 1st- and 2nd-order sensitivities need to be computed and included in any methodology that combines computational and experimental information. While the higher-order sensitivities may contribute little in special situations, e.g., when the model parameters are known with high precision, at least the 2nd-order sensitivities are needed to be included, while the 3rd-order sensitivities would be needed in order to quantitatively confirm or infirm the necessity of including sensitivities of order three and/or higher-order.

Ongoing research is dedicated to computing the best-estimate calibrated parameters, and their corresponding best-estimate reduced uncertainties, which are to be obtained by applying the 2nd-BERRU-PM methodology for the illustra-

tive example presented in this work. Once the best-estimate calibrated parameters and their accompanying best-estimate reduced uncertainties are obtained, they will enable the subsequent computations, via a corresponding forward computation using the PARTISN-software, that will produce the best-estimate responses values and their accompanying reduced uncertainties. Ongoing research also aims at extending Cacuci's 2nd-BERRU-PM [1] [2] methodology to fourth-order, thus enabling the computation of third-order response correlations (skewness) and fourth-order response correlations (kurtosis).

Conflicts of Interest

The authors declare no conflict of interest regarding the publication of this paper.

References

[1] Cacuci, D.G. (2023) Second-Order MaxEnt Predictive Modeling Methodology. I: Deterministically Incorporated Computational Model Responses (2nd-BERRU-PMD). *American Journal of Computational Mathematics.*

[2] Cacuci, D.G. (2023) Second-Order MaxEnt Predictive Modelling Methodology. II: Probabilistically Incorporated Computational Model (2nd-BERRU-PMP). *American Journal of Computational Mathematics.*

[3] Jaynes, E.T. (1957) Information Theory and Statistical Mechanics. *Physical Review Journals Archive*, **106**, 620-630. https://doi.org/10.1103/PhysRev.106.620

[4] Shannon, C.E. (1948) A Mathematical Theory of Communication. *The Bell System Technical Journal*, **27**, 379-423. https://doi.org/10.1002/j.1538-7305.1948.tb01338.x

[5] Lewis, J.M., Lakshmivarahan, S. and Dhall, S.K. (2006) Dynamic Data Assimilation: A Least Square Approach. Cambridge University Press, Cambridge. https://doi.org/10.1017/CBO9780511526480

[6] Valentine, T.E. (2006) Polyethylene-Reflected Plutonium Metal Sphere Subcritical Noise Measurements, SUB-PU-METMIXED-001. International Handbook of Evaluated Criticality Safety Benchmark Experiments, NEA/NSC/DOC(95)03/I-IX, Organization for Economic Co-Operation and Development, Nuclear Energy Agency, Paris.

[7] Alcouffe, R.E., Baker, R.S., Dahl, J.A., Turner, S.A. and Ward, R. (2008) PARTISN: A Time-Dependent, Parallel Neutral Particle Transport Code System. Los Alamos National Laboratory, Los Alamos.

[8] Wilson, W.B., Perry, R.T., Shores, E.F., Charlton, W.S., Parish, T.A., Estes, G.P., Brown, T.H., Arthur, E.D., Bozoian, M., England, T.R., *et al.* (2002) SOURCES 4C: A Code for Calculating (α, n), Spontaneous Fission, and Delayed Neutron Sources and Spectra. *Proceedings of the American Nuclear Society/Radiation Protection and Shielding Division* 12*th Biennial Topical Meeting*, Santa Fe, 14-18 April 2002.

[9] Conlin, J.L., Parsons, D.K., Gardiner, S.J., Beth Lee, M.G.M. and White, M.C. (2013) MENDF71X: Multigroup Neutron Cross-Section Data Tables Based upon ENDF/B-VII.1X. Los Alamos National Laboratory Report LA-UR-15-29571, Los Alamos National Laboratory, Los Alamos.

[10] Cacuci, D.G. and Fang, R. (2023) The nth-Order Comprehensive Adjoint Sensitivity Analysis Methodology, Volume II: Overcoming the Curse of Dimensionality: Large-Scale Application. Springer, Cham. https://doi.org/10.1007/978-3-031-19635-5

[11] Fang, R. and Cacuci, D.G. (2022) Fourth-Order Adjoint Sensitivity and Uncertainty Analysis of an OECD/NEA Reactor Physics Benchmark: II. Computed Response Uncertainties. *Journal of Nuclear Engineering*, **3**, 1-16. https://doi.org/10.3390/jne3010001

[12] Cacuci, D.G. and Fang, R. (2021) Fourth-Order Adjoint Sensitivity Analysis of an OECD/NEA Reactor Physics Benchmark: I. Mathematical Expressions and CPU-Time Comparisons for Computing 1st-, 2nd- and 3rd-Order Sensitivities. *American Journal of Computational Mathematics*, **11**, 94-132. https://doi.org/10.4236/ajcm.2021.112009

[13] Cacuci, D.G. and Fang, R. (2021) Fourth-Order Adjoint Sensitivity Analysis of an OECD/NEA Reactor Physics Benchmark: II. Mathematical Expressions and CPU-Time Comparisons for Computing 4th-Order Sensitivities. *American Journal of Computational Mathematics*, **11**, 133-156. https://doi.org/10.4236/ajcm.2021.112010